

# Sediment source, turbidity maximum, and implications for mud exchange between channel and mangroves in an Amazonian estuary

Nils Edvin Asp<sup>1</sup> · Vando José Costa Gomes<sup>2</sup> · Andrea Ogston<sup>3</sup> · José Carlos Corrêa Borges<sup>4</sup> · Charles Albert Nittrouer<sup>3</sup>

Received: 3 July 2015 / Accepted: 7 December 2015 / Published online: 14 January 2016  
© Springer-Verlag Berlin Heidelberg 2016

**Abstract** The tide-dominated eastern sector of the Brazilian Amazonian coast includes large mangrove areas and several estuaries, including the estuary associated with the Urumajó River. There, the dynamics of suspended sediments and delivery mechanisms for mud to the tidal flats and mangroves are complex and were investigated in this study. Four longitudinal

measuring campaigns were carried out, encompassing spring/neap tides and dry/rainy seasons. During spring tides, water levels were measured simultaneously at 5 points along the estuary. Currents, salinity, and suspended sediment concentrations (SSCs) were measured over the tidal cycle in a cross section at the middle sector of the estuary. Results show a marked turbidity maximum zone (TMZ) during the rainy season, with a 4-km upstream displacement from neap to spring tide. During dry season, the TMZ was conspicuous only during neap tide and dislocated about 5 km upstream and was substantially less apparent in comparison to that observed during rainy season. The results show that mud is being concentrated in the channel associated with the TMZ especially during the rainy season. At this time, a substantial amount of the mud is washed out from mangroves to the estuarine channel and hydrodynamic/salinity conditions for TMZ formation are optimal. As expected, transport to the mangrove flats is most effective during spring tide and substantially reduced at neap tide, when mangroves are not being flooded. During the dry season, mud is resuspended from the bed in the TMZ sector and is a source of sediment delivered to the tidal flats and mangroves. The seasonal variation of the sediments on the seabed is in agreement with the variation of suspended sediments as well.

---

Responsible Editor: Carlos Augusto França Schettini

This article is part of the Topical Collection on *Physics of Estuaries and Coastal Seas 2014 in Porto de Galinhas, PE, Brazil, 19–23 October 2014*

✉ Nils Edvin Asp  
nilsasp@ufpa.br

Vando José Costa Gomes  
vandojcg@yahoo.com.br

Andrea Ogston  
ogston@ocean.washington.edu

José Carlos Corrêa Borges  
carlos14.cn@gmail.com

Charles Albert Nittrouer  
nittroue@ocean.washington.edu

<sup>1</sup> Institute for Coastal Studies, Federal University of Pará (UFPA), Alameda Leandro Ribeiro, s/n – Bairro Aldeia Campus UFPA Bragança, Bragança, PA CEP 68600-000, Brazil

<sup>2</sup> PPG on Environmental Biology (PPBA), Federal University of Pará (UFPA), Alameda Leandro Ribeiro, s/n – Bairro Aldeia Campus UFPA Bragança, Bragança, PA CEP 68600-000, Brazil

<sup>3</sup> School of Oceanography, University of Washington, Box 357940, Seattle, WA 98195-7940, USA

<sup>4</sup> Natural Sciences Faculty, Federal University of Pará (UFPA), Alameda Leandro Ribeiro, s/n – Bairro Aldeia Campus UFPA Bragança, Bragança, PA CEP 68600-000, Brazil

**Keywords** Macrotidal estuaries · Suspended-sediment transport · Tidal and seasonal variation · Mud transport

## 1 Introduction

The tide-dominated eastern sector of the Brazilian Amazonian coast includes large mangrove areas and several estuaries, including the estuary of the Urumajó River. The sediment dynamics and exchange between the inner shelf, estuarine basins, and

muddy plains are not well understood, particularly in terms of the role played by the turbidity maximum zone (TMZ). As pointed out by Dyer (1997), turbidity maxima are one of the most distinctive features in both partially and well-mixed estuaries. Although turbidity maxima are discernible in satellite images for several different Amazonian estuaries, these features have barely been studied in the region previously.

At the Urumajó estuary, bed sediments are mainly sands. Facies gradually change from fine sands of tidal bars near the mouth to coarse sands of alluvial origin upstream, as defined by the tidal-dominated conceptual model of facies distribution in estuaries (Dalrymple et al. 1992). Considering the geomorphologic aspects as well as the sedimentary facies, the Urumajó estuary remarkably exemplifies the tidal-dominated end-member case. On the tidal plains, muddy sediments prevail. There, mud settles extensively within the intertidal zone as the estuary fills in, resulting in a widespread ~5-m-thick mud layer associated with massive mangrove occurrence and encompassing an area of 7600 km<sup>2</sup> of continuous mangrove forests (Souza Filho et al. 2009).

The direct sources of mud deposited along this coastal region remain unclear, as the local fluvial systems, which empty in this sector forming the estuaries, are well-known as black-water rivers (Duncan and Fernandes 2010), with mean suspended sediment concentrations (SSCs) of few milligrams per liter. The Caeté River, which empties in the Caeté Bight together with the Urumajó River and has the same geological and hydrological characteristics, carries a mean SSC of about 0.003 g L<sup>-1</sup>, reaching ~0.02 g L<sup>-1</sup> during massive rainfall events, which is still a relatively low concentration compared to the estuarine portion (Castro 2011; Asp et al. 2013). Thus, it has been assumed that the Amazon River is the primary source

(Souza Filho et al. 2009), although the mechanisms of south-eastward transport of the Amazonian muds are not understood yet. Nevertheless, Nittrouer et al. (1995) have shown that during August to November, the retroflexion of the North Brazil Current (NBC) could result in a southeastward delivery of mud along the shelf, which could reach the coast. In this context, the mechanisms of transport and retention of mud in the estuaries of the eastern sector of the Amazonian coast are especially relevant to the mangrove settlement and progradation, as local fluvial sources of mud are scarce and the supply of mud from the Amazon River is uncertain.

Despite the relevance of the estuaries and mangrove belt along the coastal region, basic knowledge of tidal propagation, suspended-sediment dynamics, and salinity variation is still missing and these factors impact the delivery of sediment to the vast muddy plains. Important studies on these topics were developed close to the Amazon River mouth (e.g., Nittrouer et al. 1995; Allison et al. 2000; Allison and Lee 2004), and several efforts have taken place in the last years to address this lack of knowledge for the eastern sector of the Amazonian coast (e.g., Souza Filho et al. 2009; Silva et al. 2009; Asp et al. 2012). The present work investigates the spatial and temporal variations of suspended sediments along the Urumajó estuary (Pará State, Brazil), which is used as a natural laboratory to understand SSC dynamics of the about 23 estuaries within this region.

### 1.1 Study area

At the tide-dominated eastern sector of the Brazilian Amazonian coast, mangroves cover most of the coastal plains along its 480-km extent (Fig. 1). The mangroves of the area are

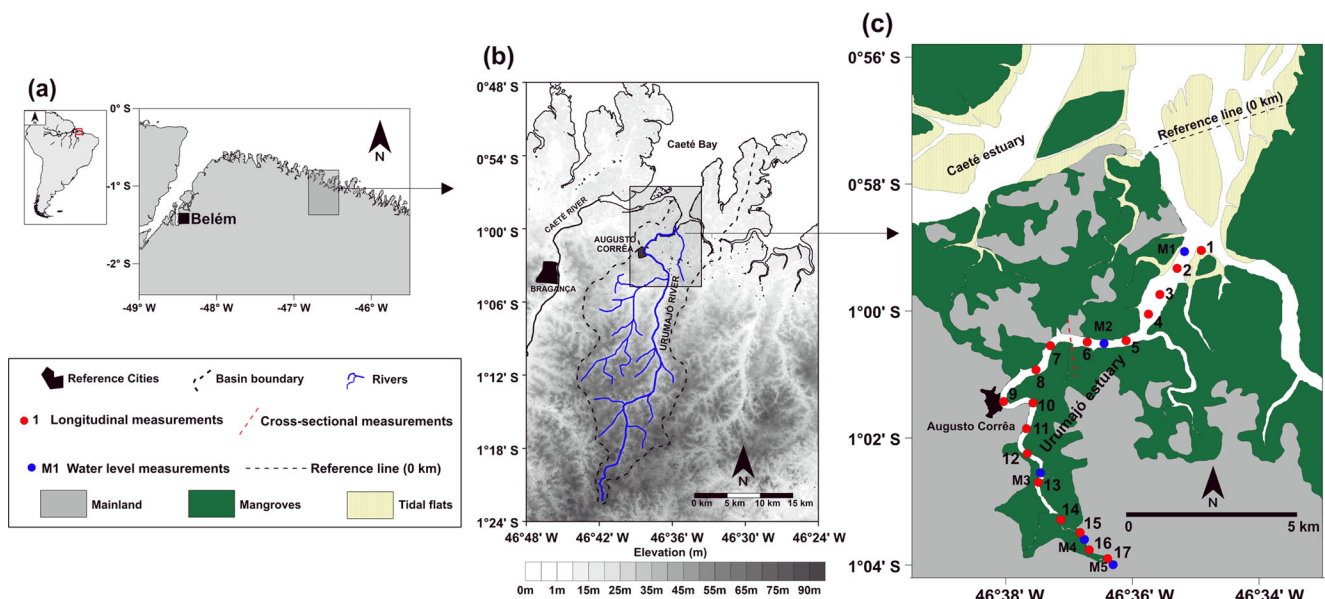


**Fig. 1** The study site, including general location (a), hydrology and topography of the Urumajó river basin (b), and Urumajó estuary with sampling locations (c)

largely dominated by two truly mangrove arboreal species, namely *Rizophora mangle* and *Avicennia germinans*. Further, the abundance of *Laguncularia racemosa* is also related with the sedimentary characteristics (Mehlig et al. 2010). Depending on the local morphodynamics, substantial sediment distribution differences are observed along the mangroves at the region. Results of Gomes et al. (2013a, 2013b), on the basis of 47 sampling sites, show that surface sediments of the area are mainly composed by silt (59 %), with 21 % sand and 20 % clay, where *Rizophora* prevails in silty areas and *Avicennia* seem to prefer clayey areas. According to topographic measurements, most mangrove areas of the region present surfaces typically 2 m higher than mean water level, which corresponds to the mean high water, being higher than typical neap tide high water (1.5 m) and substantially lower than the mean spring tide high water (2.6 m). Therefore, mangroves are flooded mainly during spring tides.

The climate in the region is controlled mainly by seasonal changes in the position of the inter-tropical convergence zone (ITCZ), which stays at latitudes of  $\sim 14^\circ$  N during August and September, migrating southwards to  $\sim 2^\circ$  S during March and April (Souza Filho et al. 2009). Therefore, the region experiences high precipitation in the first months of the year, with 73 % of the total rainfall from January to April, while September, October, and November are especially dry months (Moraes et al. 2005). Nevertheless, the air and water temperatures do not change substantially, as expected for such an equatorial coastal area. The annual regional rainfall is high, contributing to estuarine development, and ranges from 2300 to 2800 mm (Moraes et al. 2005).

The tides in the adjacent ocean have an energetic character on the Amazon shelf (Beardsley et al. 1995) and are dominated by semidiurnal tidal components. In addition to semidiurnal fluctuations of tidal processes, a distinct spring/neap modulation is produced by interaction of the components (Nittrouer et al. 1995). The typical spring tidal range at the coast is  $\sim 5$ – $6$  m, whereas during neap tides, it is  $\sim 3$  m, resulting in tidal currents frequently  $> 2$  m  $s^{-1}$  (Asp et al. 2012, 2013). Wind-generated waves reach the region mainly from the east and northeast, with dominant wave heights being 1–3 m and most energetic waves approaching the region during the southern hemisphere summer months, based on an 11-year time series obtained from the NWW3 operational model hindcast reanalysis (Pianca et al. 2010). Furthermore, measurements have showed that typical significant wave height is about 1 m at this coastal sector, where they are substantially modulated by tides, as inter- and sub-tidal banks dissipate wave energy during lower water levels. Wave periods ranged from 2 (low tide) to 12 s (high tide), associated to wave heights between 0.1 (low tide) and 1.5 m during high tide (Pereira et al. 2013).

The coastal area investigated has multiple peninsulas separated by  $\sim 23$  estuaries (Souza Filho et al. 2009), including the

Urumajó estuary (Fig. 1), resulting in a complex intercalation of coastal plain peninsulas and estuarine embayments. Due to the frictional effects of the strong tidal currents in relative shallow estuaries, resulting in turbulent flow, the estuaries are generally well-mixed, while substantially increased fluvial discharges during the rainy season may result in partially mixed conditions (Asp et al. 2013). Specifically, the Urumajó is rather well-mixed, as the tidal range is  $> 5$  m and the estuary is shallow ( $\sim 4$ – $6$  m).

Considering the scales in the Amazonian basin, the Urumajó River is small, with a drainage basin of about 544 km<sup>2</sup> and a length of  $\sim 70$  km, where the tidal influence reaches as far as 30 km upstream. There are no regular or historical measurements of fluvial discharge by the Urumajó River. However, our measurements over the last 5 years indicate that its mean fluvial discharge is about 10 m<sup>3</sup> s<sup>-1</sup>, ranging from practically zero during the driest months (September–October) to about 40 m<sup>3</sup> s<sup>-1</sup> during April (March–May). This contrasts with a tidal range of more than 5 m during spring tides and typically 3 m during neap tides, resulting in instantaneous discharges of up to 800 m<sup>3</sup> s<sup>-1</sup> in the middle estuary. Thus, the hydrodynamic processes are mainly tidal-driven and the estuary as a whole is clearly a tide-dominated end-member case, as mentioned previously. Its small dimensions are desirable characteristics in the context of this study, as measurements representing an instantaneous picture of the entire estuary are feasible at this scale.

## 2 Methods

Four measurement campaigns were carried out along the estuary, including spring and neap tidal conditions, encompassing low and high fluvial discharge periods at the rainy (January–June) and dry season (July–December). Low discharge measurements were carried out during December 2012. As the rainy seasons of 2013 and 2014 presented precipitation rates substantially lower than the historical average, the measurements corresponding to high fluvial discharge were done in May 2015.

Salinity (i.e., conductivity and temperature) and turbidity were measured from surface to the bottom with a conductivity, temperature, and depth (CTD) probe (CTD90M Sea&Sun Technology, including a Seapoint turbidity meter) at 17 stations, spaced about 1 km apart using a small, fast boat with the flood tidal phase. Simultaneous to the CTD vertical profiling, water samples were taken at surface ( $\sim 0.30$  m beneath it) and close to the bottom ( $\sim 1$  m above it), to perform SSC calibrations. Additionally, during spring tides (dry and rainy seasons), bottom sediments were sampled at each station using a 3-L Petersen grab. The grain-size distribution was analyzed with regular techniques based on sieving at 1/4 phi interval (coarse fraction) and settling velocities/Stokes' law (fine

fraction), including prior removal of salt and organic matter. During the spring-tide measurements, water levels were carried out simultaneously at five (dry season) and four (rainy season) positions along the estuary (at ~6, 8, 16, 19, and 21 km from the mouth, as defined in Fig. 1) using pressure sensors/data loggers (HOBO U20-002-Ti Onset) that recorded data every 5 min. As it was not possible to reference water levels to a published datum, they were referred to the mean water level of the outermost measurement point. Upstream measurements were adjusted to the high water of the outermost measurement, and elevations are not absolute.

For a better perspective of tide-driven dynamics, additional measurements were performed during entire tidal cycles at a cross section located about 9 km from the mouth, including current velocities with an ADCP (1200 kHz Teledyne workhorse monitor), water levels, turbidity, and salinity. Data collection alternated between ADCP cross sections and CTD vertical profiling approximately every 30 min. Along with the CTD profiling, water samples were taken at surface and close to the bottom as well. SSCs were obtained from filtering of the water samples (APHA 1995), and results were further related to the turbidity data. Several tests were performed and the best fit to the trend of the data was obtained using a polynomial correlation of second order ( $R^2=0.962$ ), as showed in Fig. 2.

As SSC is naturally high in the Amazonian estuaries and a concentration of up to  $0.25 \text{ g L}^{-1}$  might be common (Asp et al. 2013), a value of  $0.3 \text{ g L}^{-1}$  was considered to refer to high concentrations and therefore to characterize TMZs.

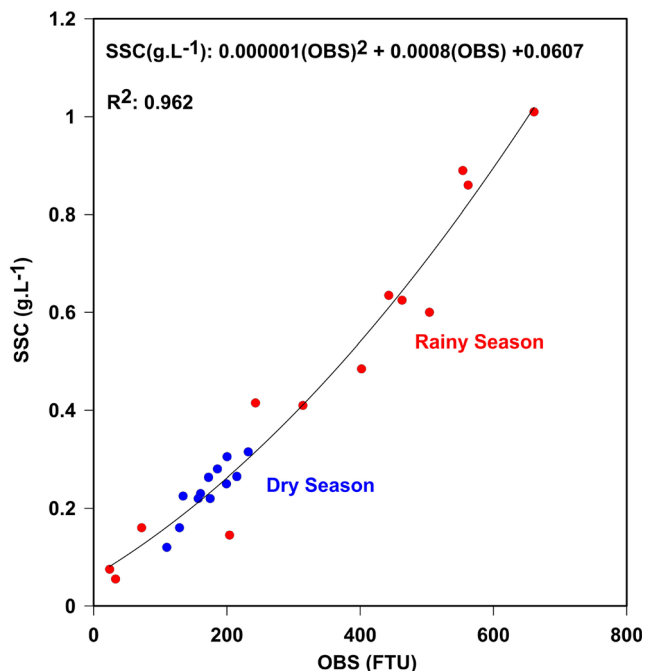


**Fig. 2** Correlation between turbidity and suspended sediment concentration (SSC) and the resulting calibration equation

## 3 Results

### 3.1 Longitudinal tidal variation

On the basis of water level measurements along the estuary in September 2013 (dry season) and May 2015 (rainy season), the propagation of the tide was evaluated (Fig. 3). During the dry season, it is observed that at the outermost part of the estuary (0–8 km from the mouth), the tide experienced a very slight amplification. Farther upstream (middle sector, 8–16 km from the mouth), a substantial attenuation is observed at the same time that asymmetry increased. At the transition from the middle to the uppermost sector (16–19 km from the mouth), there is a relative stabilization of the attenuation/deformation of the tide wave, followed by a strong new increase in the asymmetry and attenuation farther upstream.

During the rainy season, there is a remarkable attenuation of the tide starting at the mouth. The rate of attenuation is reduced in the middle sector and increases again in the uppermost part of the estuary. In this situation, the asymmetry of the tide seems to increase exponentially from the mouth to the estuarine head under high discharge. Mean flood duration was 5.7 h in the dry and 5.2 h in the rainy season. Therefore, the ebb phase took on average 6.7 h during dry and 7.2 h during the rainy season.

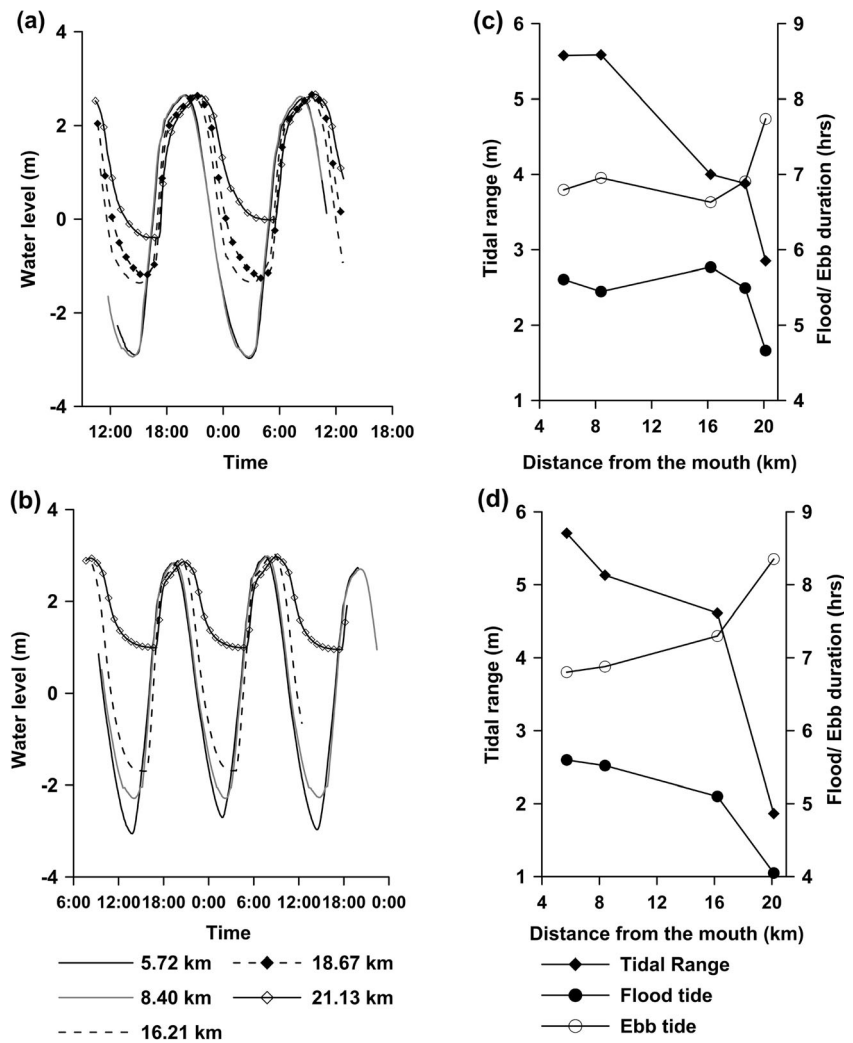
During the dry season, the attenuation experienced by the tide was regular upstream of the outermost, funnel-shaped sector, dropping from 5.65 to 4.00 m between km 8 and km 16 ( $0.21 \text{ m km}^{-1}$ ) and from 4.00 to 2.80 m between km 16 and km 21 ( $0.24 \text{ m km}^{-1}$ ). During the rainy season, the attenuation and increasing asymmetry were observed all along the estuary, but in this case, both asymmetry and attenuation were most remarkable at the upper estuary. Tidal range dropped from 5.70 to 4.55 m between km 6 and km 16 ( $0.115 \text{ m km}^{-1}$ ) and from 4.55 to 1.90 m between km 16 and km 21 ( $0.53 \text{ m km}^{-1}$ ).

Regarding the longitudinal variation of SSC, it is of note that spring-neap diurnal differences and dry-rainy seasonal differences are similar. A single comparison of mean values and ratios between them gives a general picture of the patterns (Table 1). Mean SSC during spring tides is almost three times greater than during neap tides in both seasonal periods. On the other hand, mean SSC during the rainy season is also almost three times bigger than during the dry season. The ratios of spring to neap tide (independent of season) and of rainy to dry season (independent of tide) are between 2.5 and 3.

When longitudinal and vertical variation of SSC in conjunction with salinity is considered, the formation of a TMZ is evident, especially during the rainy season. In this period, mean SSC was about  $0.81 \text{ g L}^{-1}$  for spring tide and about  $0.31 \text{ g L}^{-1}$  for neap tide. The SSC reached  $1.23 \text{ g L}^{-1}$  at 13 to 15 km from the mouth and  $0.7 \text{ g L}^{-1}$  at 12 to 14 km from the mouth, under spring and neap conditions respectively,



**Fig. 3** Water level oscillation along the Urumajó estuary based on simultaneous measurements at five locations. **a, b** Oscillation during dry and rainy seasons, respectively. **c, d** Longitudinal variation of tidal range and duration of tidal phases during dry and rainy seasons, respectively, on the basis of measured water levels. Note that at ~17 km from the mouth, there is an important pattern change



coinciding with low values of salinity (e.g., <5 for neap and <10 for spring tide), as shown in Figs. 4 and 5.

As expected, the salt intrusion increases with the increase of tidal range and reduction of fluvial discharge. Therefore, a salinity of up to 20 is found 20 km upstream of the mouth during dry season/spring tide and a salinity of 12 was measured at the estuary mouth during rainy season/neap tide (all

measurements were performed by the end of flood; Figs. 4 and 5).

Bottom sediment samples obtained at the 17 CTD stations during the dry and rainy stations under spring-tide conditions showed substantial seasonal variation and provided a significant means to comprehend the suspended-sediment dynamics. In general, during the rainy season, the mud content in the bottom samples was much higher. On average of the 17 samples, the sediments were composed of 7 % of gravel, 72 % sand, and 21 % mud during the dry season. In contrast, during the rainy season, the mean values were 4 % for gravel, 57 % for sand, and 39 % for mud (Fig. 6).

Despite the seasonal changes, there are some persistent longitudinal variations in grain size. The outer part (i.e., km 0–8) is characterized mainly by fine to very fine sands from the inner shelf (mean grain size of 2.1 to 3.2 Phi). At the middle sector (km 8–16), there is a mixture of coarse sands of fluvial origin, with some amount of the fine sands from the ocean, and the estuarine fine sediments. At the uppermost sector (16–19 km), fluvial coarse sands are dominant.

**Table 1** Mean SSC of longitudinal measurements and ratios between different conditions

Synodic variation	Seasonal variation	Mean SSC (g/L <sup>-1</sup> )	Ratio
Spring tide	Rainy season	0.813	2.90
Spring tide	Dry season	0.281	
Neap tide	Rainy season	0.314	2.98
Neap tide	Dry season	0.105	
Spring tide (dry-rainy seasonal average)		0.547	2.61
Neap tide (dry-rainy seasonal average)		0.209	
Rainy season (spring-neap tide average)		0.563	2.92
Dry season (spring-neap tide average)		0.193	

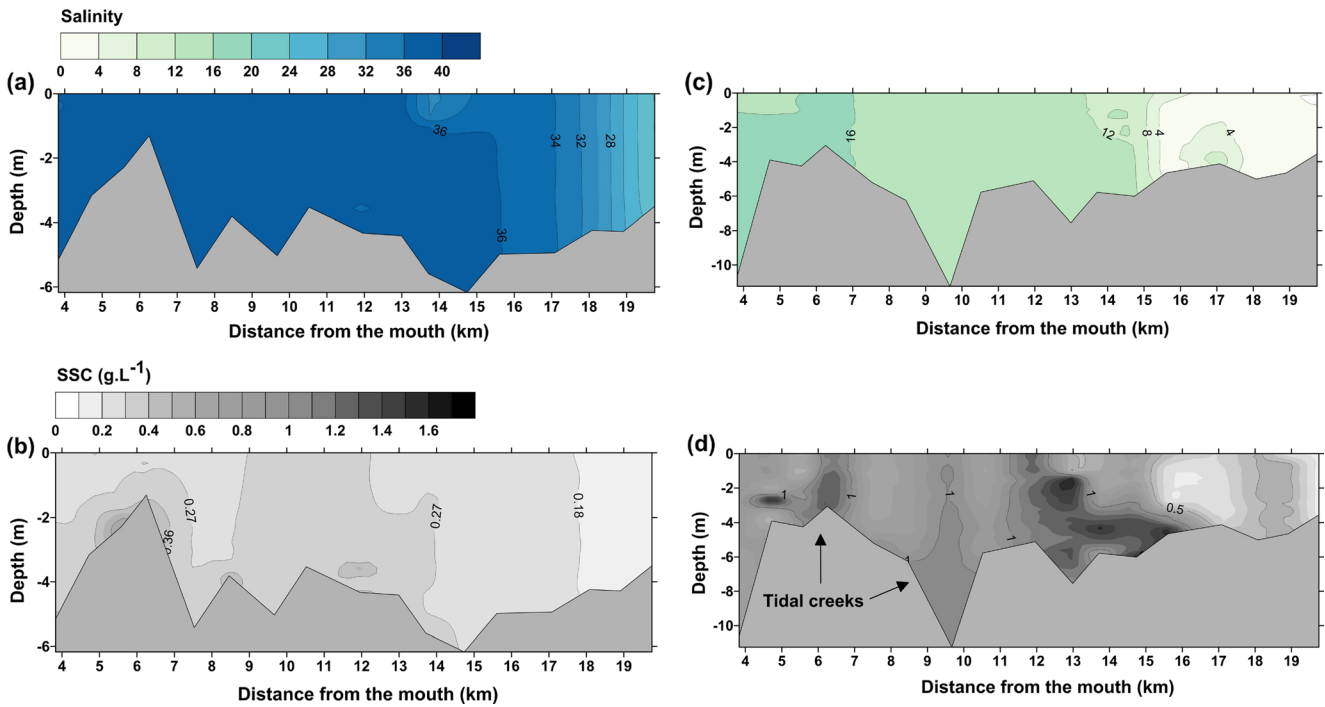


Fig. 4 Longitudinal and vertical variation of salinity and SSC under spring-tide conditions, during dry (a, b) and rainy (c, d) seasons

When the longitudinal and seasonal variation of bottom sediments is compared to the SSC at surface, it indicates that more mud has been deposited on the bottom during the rainy season. Mean SSC at surface is greater during dry season, although vertical measurements indicate greater SSC near the bed during rainy season.

Two seabed areas of mud concentration are observed during the rainy season, possibly reflected the regions of the TMZ during spring and neap conditions, with a shift of 2 to 5 km. During the dry season, this correlation is not clear, where basically one area of seabed mud concentration is observed and the TMZ was not conspicuous.

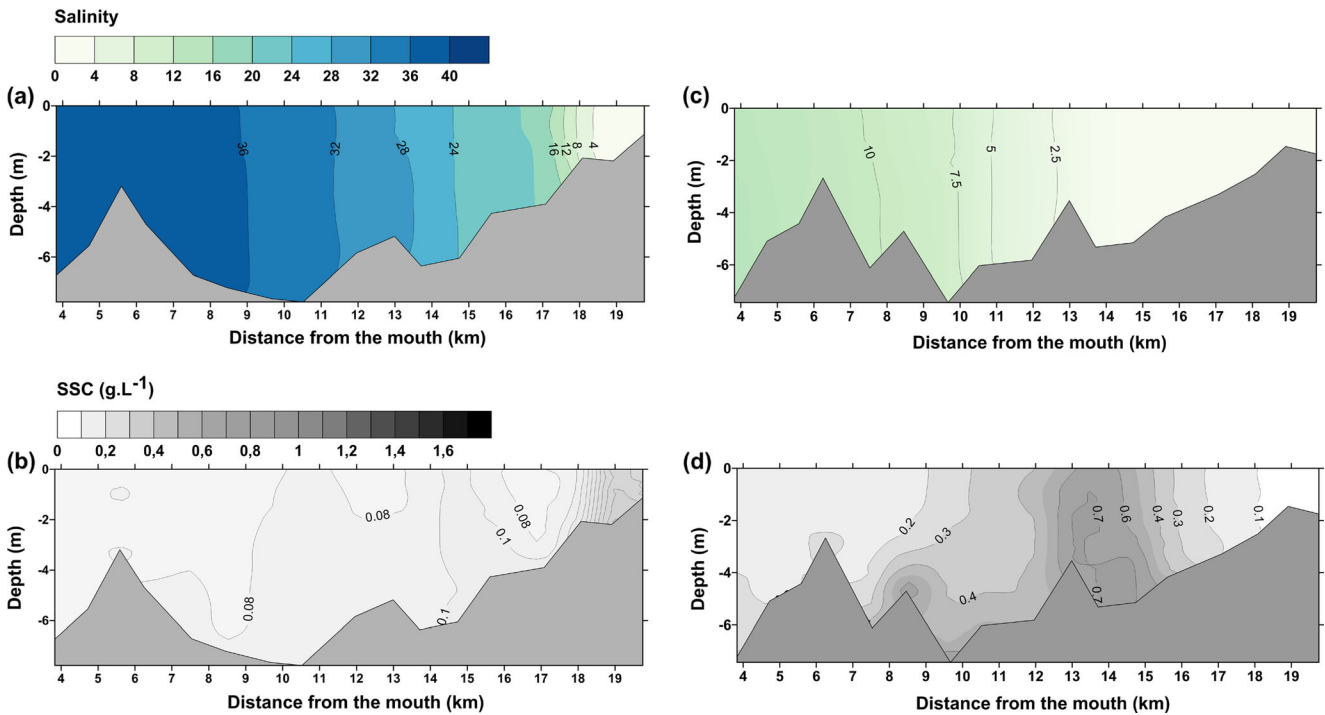
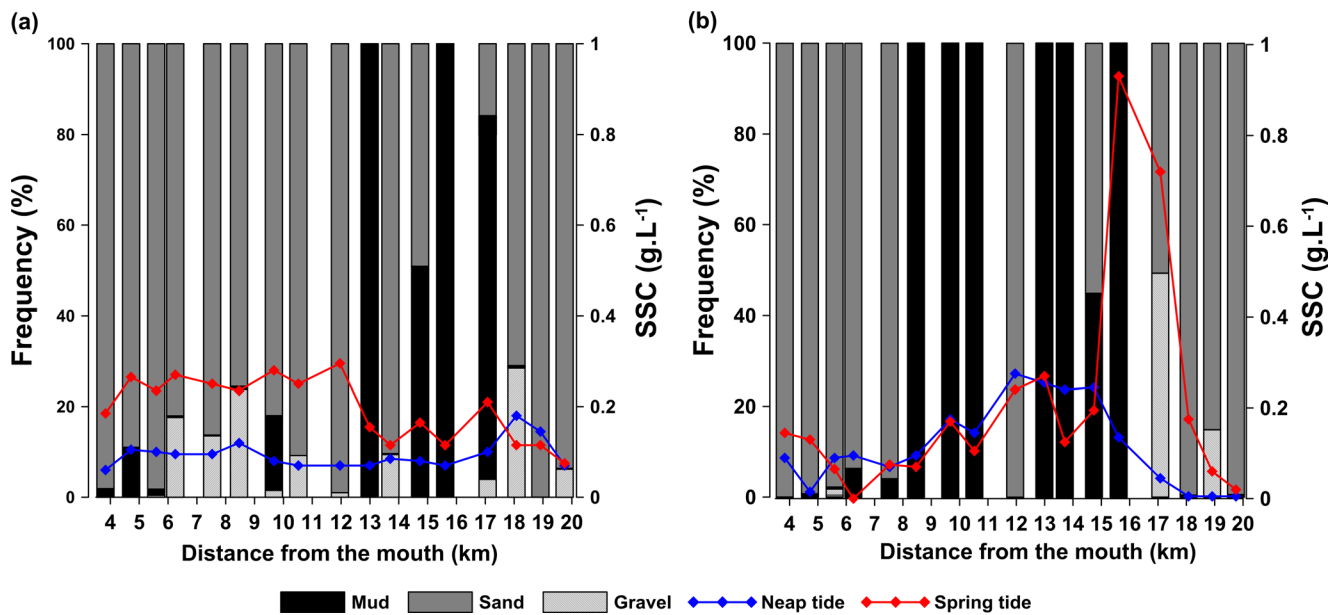


Fig. 5 Longitudinal and vertical variation of salinity and SSC under neap-tide conditions, during dry (a, b) and rainy (c, d) seasons



**Fig. 6** Longitudinal variation of bottom sediments during dry (a) and rainy (b) seasons, along with SSC at the sea surface. Note that results presented in each panel were collected simultaneously during December 2012 and April 2013, respectively

### 3.2 Tidal cycle variation on the cross-sectional basis

The monitored cross section is situated 9 km upstream of the estuarine mouth, within the outer half of the middle sector of the estuary. As a result of the increased discharge during the rainy season, the asymmetry of the water level variation increased from dry to rainy periods. The duration of the flood phase was 5.17 h, and the ebb phase was 7.23 h during the dry season. During the rainy season, the ebb duration was 7.75 h and the flood lasted 4.65 h (Fig. 7).

The tidal range at the monitored cross section was around 5.42 m during the dry season and around 4.73 m during the rainy season (Fig. 7). This difference is the combined effect of the fluvial discharge with the astronomic signal itself, as the predicted tidal range at the coast during the measurements of the rainy season was of 5.2 m, while the predicted tidal range during the measurements of the rainy season was 4.5 m (DHN 2015). These results are in agreement with the tidal propagation and its seasonal variation, presented in Fig. 3, where from the outer to the middle sector of the estuary there is a slight amplification and asymmetry reduction during the dry period. In contrast during the rainy season, there is a significant tidal attenuation and asymmetry increase in this portion of the estuary.

The tidal-fluvial flows in terms of discharge and current velocities clearly express the increase of the fluvial discharge. During the dry season, the pattern is almost exclusively related to the tidal asymmetry, where instantaneous maximum discharges ( $790 \text{ m}^3 \text{ s}^{-1}$ ) and velocities ( $1.18 \text{ m s}^{-1}$ ) are reached during the flood and are slightly greater than during the ebb phase, with a maximum instantaneous discharge of  $775 \text{ m}^3 \text{ s}^{-1}$

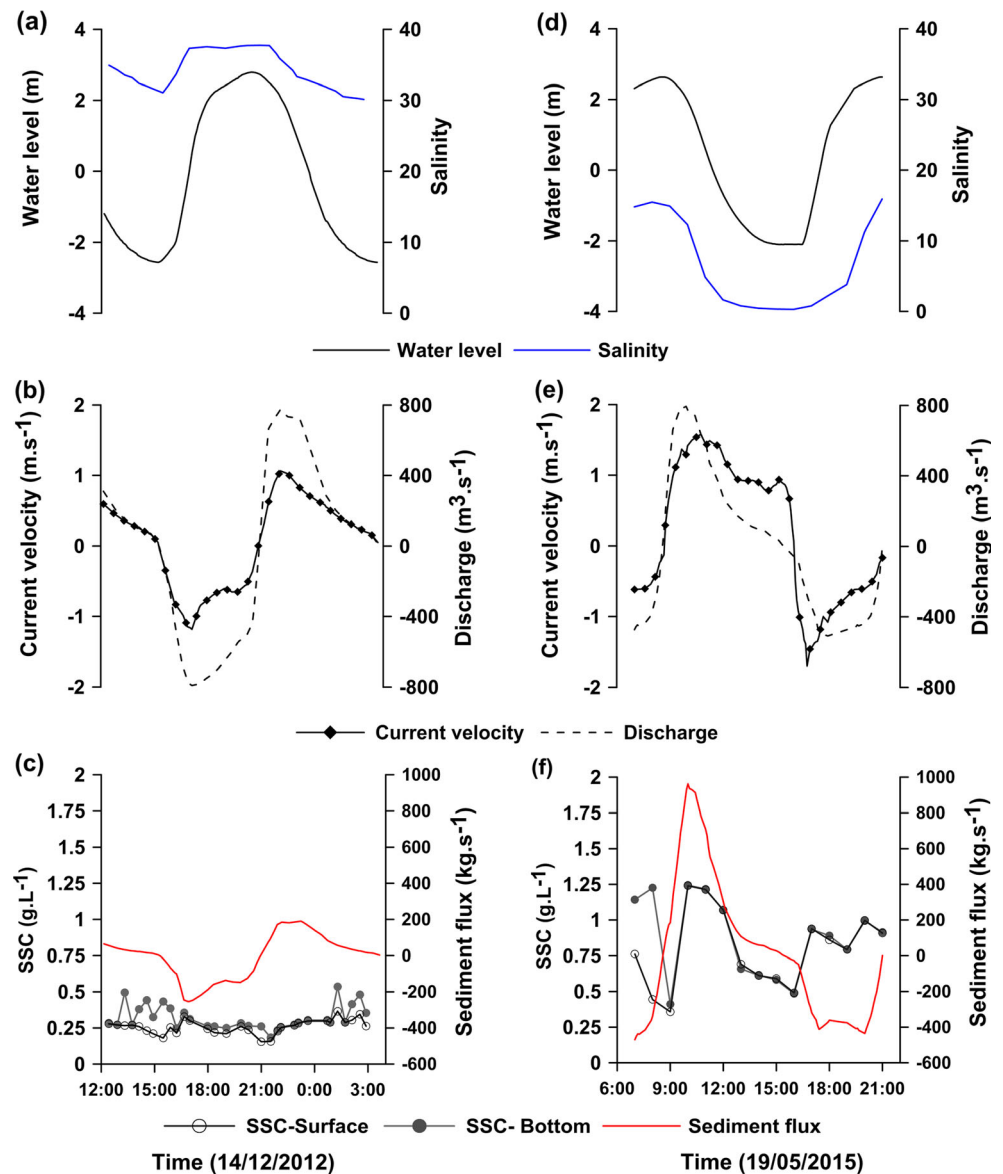
and velocity of  $1.06 \text{ m s}^{-1}$  (Fig. 7). During the rainy period, the increased fluvial discharge resulted in a substantial increment in the tidal asymmetry of flow and in the current velocities as a whole. Maximum instantaneous discharges were  $509 \text{ m}^3 \text{ s}^{-1}$  for the flood and  $794 \text{ m}^3 \text{ s}^{-1}$  for the ebb phase, whereas the maximum, cross-sectionally averaged, instantaneous current velocities were  $1.37 \text{ m s}^{-1}$  for the ebb and  $1.70 \text{ m s}^{-1}$  for the flood phase.

As expected, the very low fluvial discharge during the dry season resulted in high salinities, reaching 37.7 at high water and 31.0 during low water. Vertical (surface-bottom) differences were discernible only at the end of ebb phase and even so were smaller than 1. During the rainy season, maximum salinity was 15.9 and minimum was 0.3, mirroring the water level fluctuation (Fig. 7). Surface-bottom differences were smaller than 0.2. The depth-averaged salinity is presented in Fig. 7.

Comparing the water level with the current velocity variation throughout the tidal cycle of dry and rainy periods, it becomes clear that velocities are much higher during rainy season, when the asymmetric propagation of the tide results in a sudden and substantial increase in the velocity at the beginning of the flood (Fig. 8). During dry season, this increase of velocity is rather gradual during the flood, reaching maximum values close to the middle of the phase, gradually decaying towards high water.

During the ebb of the rainy season, a substantial increase of velocities is observed right at the beginning of the tidal phase, decaying gradually after that. A similar pattern is observed at the ebb of the dry period, although with significantly lower velocities (Fig. 8). It is important to note that at water

**Fig. 7** Hydrodynamics at the monitored cross section comparing spring tides during dry (a–c) and rainy (d–f) periods. Water level and depth-averaged salinity are presented in a and d; discharge and velocity are presented in b and e, whereas SSC is presented at c and f



elevations of  $\sim 2.1$  m, the mangrove forests are being effectively flooded.

The effects of the very low discharge of the Urumajó River during the dry season as well as of its substantial increase during the rainy season are very conspicuous in the salinity measurements at the cross section as well. During dry period, salinity varied from 30 during the low water and reached 37 during high water. During the rainy period, salinity was close to zero at low water and reached 17 during high water.

The SSC during the rainy season was significantly greater than during the dry season, resembling the longitudinal measurements with a ratio of 3 to 1 (rainy to dry season SSC) again. On the other hand, mean values show no significant differences of SSC between ebb and flood phases in each seasonal period. The mean SSC during the dry season was  $0.25 \text{ g L}^{-1}$  in both tidal phases. During the rainy period, mean

SSC was  $0.74 \text{ g L}^{-1}$  for the flood and  $0.78 \text{ g L}^{-1}$  for the ebb phase (Fig. 7). Comparisons of depth-averaged SSC with the progression of the tidal cycle, expressed in terms of water level, show important ebb-flood tide and dry-rainy period variations (Fig. 9). During the dry season, it is observed that resuspension is substantial, where maximum SSC was reached in conjunction with maximum velocities, which coincides with the beginning of the ebb (lower water levels) and middle of the flood (intermediate water levels), as showed at Fig. 9a. Furthermore, it is evident that SSC is substantially lower at the beginning of the ebb in relation to the end of the flood.

The “behavior” of SSC during the rainy period differs substantially from that of dry season. At both low and high water levels, concentrations are similar at ebb and flood phases. However, at intermediate water levels, there is a substantial



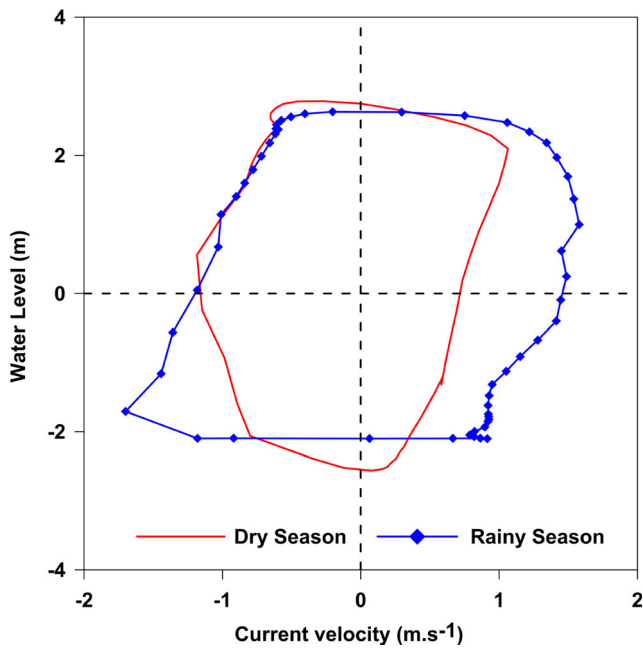


**Fig. 8** Relationship between water level and current velocity on the basis of cross-sectional measurements. Note that the tidal cycle advances clockwise and positive currents are in the ebb direction

reduction of SSC as flood phase advances, increasing again towards high water. During the ebb phase, there is a gradual and substantial increase of SSC, reaching a maximum value of  $1.24 \text{ g L}^{-1}$  near the mean water level and gradually decaying towards low water. This reveals the incursion of the less turbid water from the outer estuary during flood. The TMZ moves downstream during the ebb, stays at 13–15 km from the mouth by the end of flood, and reaches the monitored cross section at 9 km during the ebb.

## 4 Discussion

### 4.1 Tidal hydrodynamics in the estuary

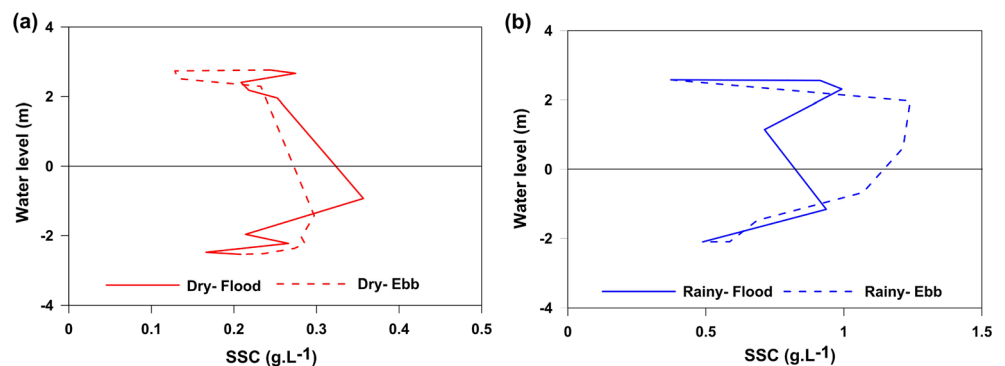
Considering the morphology and the tidal propagation along the estuary, the first 7 km of its extension (first four CTD stations in Fig. 1) was defined as the funnel-shaped outer

estuary. From the km 7 to km 16 (CTD stations 5 to 13) were considered as the middle sector, with substantial attenuation and/or deformation of the tidal wave. Upstream of km 16, it was defined as the upper estuary. Longitudinal measurements of salinity support this division, despite substantial spring-neap tide and dry-rainy season variations.

The tidal range at the monitored cross section was around 5.42 m during the dry season and around 4.73 m during the rainy season (Fig. 7). This difference is due to the combined effect of the fluvial discharge and entrance into the estuary mouth combined with the astronomic signal itself. The predicted tidal range at the coast during the measurements of the rainy season was of 5.2 m, while the predicted tidal range during the measurements of the rainy season was 4.5 m (DHN 2015). Thus, there appears to be amplification of the tide as it enters the funnel-shaped outer estuary and interacts with fluvial discharge, causing attenuation in the middle and upper sectors.

Under spring-tide conditions, the water level data show a slight tidal amplification along the first kilometers upstream of the mouth, which was attributed to the convergence (funneling effect). As the tide propagates farther into the middle sector of the estuary a gradual attenuation is observed, with no substantial increase of the asymmetry up to 17 km from the mouth. There, the ebb phase becomes progressively longer, as expected (Wang et al. 2002). In this uppermost sector, both the attenuation and the asymmetry are rapidly intensified. This increment in the attenuation and asymmetry seems to be specially related with the topography (thalweg elevation), with minor effects of funneling and fluvial discharge, as attenuation at the uppermost sector is similar during low and high discharge periods. These results suggest that the channel morphology is rather adjusted to maximum flow/current situation, which is achieved during spring tides in the rainy season. In these situations, bedload convergence (BLC) is developed, where the downstream sediment transport from the river and the ebb-dominated sediment transport of the estuary converge, as proposed by Dalrymple and Choi (2007) and testified by the bottom-sediment distribution pattern at the Urumajó (Fig. 6).

**Fig. 9** Relationship between water level and depth-averaged SSC on the basis of cross-sectional measurements. Note change in scale between the dry (a) and rainy (b) seasons



Considering the shallowness and the intensity of tidal currents, the estuary is well-mixed in both the rainy and dry seasons, as expected, showing differences between surface and near-bottom salinity <1. This seasonal and vertical pattern was also described for the well-studied neighboring Caeté estuary (Barletta-Bergan et al. 2002; Monteiro et al. 2011; Gomes et al. 2013a, b; Asp et al. 2013).

#### 4.2 Formation of the TMZ in dry and rainy seasons

Besides the longitudinal variation of the water level, the variations of salinity and especially turbidity are very relevant for the dynamics of muddy sediments and the estuary-mangrove co-evolution. During dry season, the mixed-energy sector is pushed farther upstream, even under neap-tide condition. Assuming that the channel morphology is mainly adjusted to maximum discharges during rainy season (up to 20 times greater than during dry season), there is a mismatch between hydrological and morphological ideal conditions for TMZ formation. The energy equivalency between bidirectional, flood-dominant, tidal flux, and the unidirectional river-dominated flux is reached in a narrow, shallow, and mostly turbulent sector of the estuary (Dalrymple and Choi 2007).

During dry season, a subtle TMZ may have been detected only at the neap tide but with half the concentration and longitudinal extension observed during rainy season. It is possible that the TMZ was occurring also during the spring-tide condition but out of the measured area. The seasonal variation resulted in a >5-km upstream displacement of the TMZ under neap conditions from the rainy to the dry season. Nevertheless, there is no evidence from the bottom sediment of a BLC at that sector (Fig. 6).

In general, mean SSC during spring tides and during the rainy periods was between 2.5 and 3 greater than during neap tides and dry periods, respectively (Table 1). Most of the muddy tidal flats and mangroves are flooded only during spring tides. Results from water level variation indicate that only when water level is >2 m above mean water level an overbank tide is experienced. Therefore, circulation of mud is much greater during spring tides. The effect of strong rainfalls during the rainy season results in a similar effect, washing much of the mud from the flats and mangroves.

Besides the TMZ formation in a spatial perspective, there is substantial resuspension in a temporal perspective, as greater SSCs are often associated with stronger currents here (Fig. 7) and elsewhere tidal-driven circulation inside the estuary is important, the estuary is shallow, and fluvial discharge is relatively small (Lessa and Masselink 1995; Wolanski and Spagnol 2003; Siegle et al. 2009; Schettini and Miranda 2010; Gomes et al. 2013a, b). Nevertheless, correlations of near-surface, near-bottom, and depth-averaged SSC showed low correlations ( $R^2$ ) in all cases with current velocities. In addition to the slight temporal increases of the SSC related

to resuspension, there are SSC peaks associated with tidal creeks emptying into the main channel of the estuary, as marked in Fig. 4d. This phenomenon might mask the relationship between velocity and SSC and suggest significant advection of sediment within the study area, both from the small tidal creeks and from the ocean (Caeté Bay) itself.

The distribution patterns of muddy bottom sediment mirrored the zones of TMZ formation and displacement according to seasonal and tidal variations. At the upper estuary, coarse fluvial sands prevail, whereas close to the mouth fine sands of marine origin prevail. At the middle estuary, mud content peaks are observed at the bed, corresponding to the BLC position and the TMZ at the water column. Mud content at the bed is substantially greater during rainy season, and this is consistent with the remarkable TMZ observed in this season. As a whole, the results show that the mud is being accumulated at the middle estuary associated with the TMZ during the rainy season. During the dry season, the stored mud becomes available in the middle estuary for resuspension, where it might be transported to the mangrove plains during water high stands, especially during spring tides.

As tidal-current pattern is persistently flood-dominated, mud advection from the coast is feasible in both seasonal periods. But looking at SSC variation over a tidal cycle (Fig. 9), it seems that advection is more important during dry season. During the rainy season, mud could be exported to the coast, which is prevented by the TMZ formation.

#### 4.3 Implications for sediment source to the estuary and delivery to surrounding mangrove flats

Estuaries might receive a substantial amount of sandy sediments from the inner shelf at their outer part. In tide-dominated estuaries (e.g., those at the eastern sector of the Amazonian coast), this occurs due to the migration of elongate sand bars driven by asymmetric pattern of tides with prevailing flood currents (Lambiasi 1980; Dronkers 1986; Dalrymple et al. 1992), which is also the case for the tides in the Urumajó estuary (Fig. 7a, d). The longitudinal distribution of bottom sediments (Fig. 6) as well as the pattern of tidal propagation along the estuary (Fig. 3) also support this assertion.

On the other hand, most estuaries get the muddy sediments from the rivers that enter them (Chappell 1993; Uncles et al. 2006). Alternately, some estuaries could get the majority of sediment from the ocean. Shallow estuaries tend to be flood-dominant and enhance landward near-bed transport (Friedrichs et al. 1992). However, the advection of suspended sediments into the estuary from the ocean is a more peculiar situation, as the adjacent ocean usually contains very concentrations of mud relative to the river.

The trapping mechanisms of fine sediments in estuaries and mangrove swamps have been described (e.g., Wolanski

1995), and mud advection from the ocean to the estuary is probable when SSC at the ocean (along the coast) is greater than that of a blackwater river emptying into it. In fact, at the mouth of the Urumajó estuary on the continental shelf, a turbid coastal boundary layer encompasses a ~15-km strip between the coastline and the 20-m isobath (Cavalcante et al. 2010) and might present  $SSC > 0.010 \text{ g L}^{-1}$  (DeMaster et al. 1996), which would be at least three times greater than that of the Urumajó River above tidal influence. Within the estuary, the observations show larger SSC at stations towards to estuary mouth than at stations farther upstream (Fig. 6) during the dry season with the exception of the subtle TMZ seen at the uppermost stations during neap tides, suggesting that the source of sediment is from the offshore direction. The net sediment flux during the dry season is also in the flood direction and can move sediment into the estuary at a time when there is no riverine source of sediment. During the rainy season, greater SSC within the TMZ at the middle part of the estuary and muddy sediment on the seabed suggests that the rainfall moves sediment from the flats into the channels (Fig. 7), and sediment can be exported from the estuary during this time. In general, conditions similar to those measured during the dry season are in effect much of the year, and it is likely that the net annual flux of sediment is into the estuary.

Therefore, the existence of a relevant advection of mud from the coast seems to be the case for the Urumajó and most estuaries along the eastern sector of the Amazonian coast (Silva et al. 2009; Souza Filho et al. 2009; Castro 2011; Asp et al. 2012, 2013). Ebb dominance, and therefore mud advection from the shelf, is observed in deeper estuaries and/or with large volume storage areas (Speer et al. 1990). The Urumajó is rather shallow, considering the tidal range. Thus, the ebb dominance observed at the Urumajó estuary (Fig. 7), especially during the dry season, should be the result of its large storage areas, represented by the mangroves.

Investigations on other tropical estuaries of Brazil as the Caravelas estuary, similar to the Urumajó in dimensions, morphology, and climate (Schettini and Miranda 2010; Pereira et al. 2010), showed that smaller storage areas would result in mud exportation. Estimates on the net suspended sediment transport for the Urumajó estuary showed an advection of 617 t (Ebb flow = 2296 t; flood flow 2913 t) of mud during the dry season for each tidal cycle. During the rainy season, the net transport results in the exportation of 2701 t (Ebb flow = 8319 t; flood flow 5618 t), as showed in Fig. 7c. At the Urumajó, the Amazon River would certainly provide the necessary SSC, even when the mechanisms of delivery of Amazon sediment to the eastern coastal region are neither clearly understood nor described.

With regard to the sediment transport onto the mangrove flats along the estuary, the results presented here suggest that during the dry season, spring tides flood the mangrove swamps and mud is trapped (as seen in the greater SSC during

floods than ebbs in Fig. 9a). The strong currents and the shallowness of the estuary promote continuous suspension within the channel during the dry season, maintaining the supply of sediment to be delivered to and trapped in the mangrove swamps. On the other hand, during the rainy season, some mud is washed out from tidal flats and mangrove swamps (greater SSC during ebbs than floods in Fig. 9b) and adds to sediment resuspended in the channel by tidal currents, and the TMZ appears to trap muddy sediments in the channel, promoting deposition of a muddy bed (Fig. 6b). Regionally, the eastern Amazonian coast presents estuaries with a substantial local river source including drainage basins in the order of tens of thousands square kilometers (e.g., Capim-Guamá, Freitas et al. 2012; Gurupi, Asp et al. 2013). However, it seems that the sediment yield is still small relative to the sediment storage in the drainage basin, similar to that described for other humid but sub-tropical, large drainage basins of the American Atlantic coast (Phillips 1991). For the Amazonian region, due to its low relief and tropical wet climate, this storage of sediment inside the basin is naturally very high and large forests and freshwater swamps develop in the flood plains. Indeed, much of the sediments of the Amazon River are being stored at its flood plains, especially in the lower Amazon (Nittrouer et al. 1995; Irion et al. 2010). The mangrove forests around the Urumajó River comprise the longest continuous mangrove belt of the world, and the results presented here suggest that advection of mud from the adjacent coast during the dry season and the formation of a turbidity maximum zone during the rainy season resulting from tidal processes as well as rainfall on the flats appear to be important mechanisms for the maintenance and progradation of mangroves in the area.

## 5 Conclusions

The dynamics of suspended sediments and delivery mechanisms for mud to the tidal flats and mangroves in the Urumajó estuary are complex, and the results of this study are likely applicable to the other 23 estuaries along the eastern sector of the Brazilian Amazonian coast. In the Urumajó estuary, a marked TMZ forms during the rainy season, with a 4-km upstream displacement from neap to spring tide. During dry season, the TMZ was conspicuous only during neap tide and dislocated about 5 km upstream. Mud is concentrated by the TMZ formation in the channel especially during the rainy season, when a substantial amount of the mud is washed out from mangroves to the estuarine channel and hydrodynamic/salinity conditions for TMZ formation are optimal. However, in a long-term perspective muddy, sediments must be advected from the coast, as the Urumajó is a blackwater river, as most rivers of the region, to explain the remarkable Holocene mangrove development in the area, in association with the local estuaries.

As expected, transport to the mangrove swamps is most effective during spring tide and substantially reduced at neap tide, when mangroves are not being flooded. During the dry season, mud is resuspended from the bed in the TMZ sector and is a source of sediment delivered to the tidal flats and mangroves. Temporal and spatial variations of tidal currents and SSC suggest that mud advection from the coast into the estuary is taken place persistently, although more intensively during dry season.

The results presented here suggest that advection of mud from the adjacent coast and the formation of a turbidity maximum zone during the rainy season are the most important mechanisms for the maintenance and progradation of mangroves in the area. Advection from the coast would represent the main source of muds to the estuary and mangrove swamps, especially during dry season, whereas the TMZ formation prevents mud loss during high-discharge periods of the rainy season, as well as results in mud retention of muddy sediments eventually delivered by the blackwater river.

**Acknowledgments** The authors would like to thank the *Coordenação de Aperfeiçoamento de Pessoal de Nível Superior* (CAPES—Programa Pró-Amazônia: Biodiversidade e Sustentabilidade) and *Conselho Nacional para Desenvolvimento Científico e Tecnológico* of Brazil (CNPq - 446895/2014-8) for the funding of the project and the fellowship of Nils E. Asp (CNPq - 304279/2012-9), as well as for the scholarship of José Carlos Corrêa Borges (PIBIC/CNPq).

Furthermore, Nils Asp is especially thankful to Augustus Vogel, PhD and the Office of Naval Research Global (ONRG), for the Visiting Scientist Grant, which helped substantially the writing of this manuscript during the visit at the School of Oceanography/University of Washington.

We are also thankful to all personnel of the *Laboratório de Geologia Costeira* (LAGECO) of the *Universidade Federal do Pará* (UFPA), for the assistance at the fieldwork and laboratorial analyses, as well as to the anonymous reviewers for their valuable comments and suggestions.

## References

- Allison MA, Lee MT (2004) Sediment exchange between Amazon mudbanks and shore-fringing mangroves in French Guiana. *Mar Geol* 208:169–190
- Allison MA, Lee MT, Ogston AS, Aller RC (2000) Origin of Amazon mudbanks along the northeastern coast of South America. *Mar Geol* 163:241–256
- APHA (1995) Standard methods for the examination of water and wastewater. American Public Health Association, Washington DC
- Asp NE, Schettini CAF, Siegle E, Silva MS, Brito RNR (2012) The dynamics of a frictionally-dominated Amazonian estuary. *Braz J Oceanogr* 60:391–403
- Asp NE, Freitas PTA, Gomes VJC, Gomes JD (2013) Hydrodynamic overview and seasonal variation among the estuarine diversity at the eastern sector of the Amazonian coast. *J Coast Res* SI65:1092–1097
- Barletta-Bergan A, Barletta M, Ulrich SP (2002) Structure and seasonal dynamics larval fish in the Caeté river estuary in North Brazil. *Estuar Coast Shelf Sci* 54:193–206
- Beardsley RC, Candela J, Limeburner R, Geyer WR, Lentz SJ, Castro BM, Cacchione D, Carneiro N (1995) The M2 tide on the Amazon shelf. *J Geophys Res* 100:2283–2319
- Castro MS (2011) Propagação de maré na porção superior do estuário do rio Caeté e seus limites (Amazônia Oriental, PA/Brasil). Dissertation, Universidade Federal do Pará
- Cavalcante GH, Kjerfve B, Knoppers B, Feary DA (2010) Coastal currents adjacent to the Caeté Estuary, Pará Region, North Brazil. *Estuar Coast Shelf Sci* 88:84–90
- Chappell J (1993) Contrasting Holocene sedimentary geologies of the lower Daly river, northern Australia, and lower Sepik-Ramu, Papua New Guinea. *Sediment Geol* 83:339–358
- Dalrymple RW, Choi K (2007) Morphologic and facies trends through the fluvial-marine transition in tide-dominated depositional systems: a schematic framework for environmental and sequence-stratigraphic interpretation. *Earth Sci Rev* 81:135–174
- Dalrymple RW, Zaitlin BA, Boyd R (1992) Estuarine facies model: conceptual basis and stratigraphic implications. *J Sediment Petrol* 62:1130–1146
- DeMaster DJ, Smith W, Nelson DM, Aller JY (1996) Biogeochemical processes in Amazon shelf waters: chemical distributions and uptake rates of silicon, carbon and nitrogen. *Cont Shelf Res* 16:617–643
- Dronkers J (1986) Tidal asymmetry and estuarine morphology. *Neth J Sea Res* 20:117–131
- Duncan WP, Fernandes MN (2010) Physicochemical characterization of the white, black, and clearwater rivers of the Amazon basin and its implications on the distribution of freshwater stingrays (Chondrichthyes, Potamotrygonidae). *PanamJAS* 5:454–464
- Dyer KR (1997) Estuaries: a physical introduction. Wiley, Chichester
- Freitas PTA, Silveira OFM, Asp NE (2012) Tide distortion and attenuation in an Amazonian tidal river. *Braz J Oceanogr* 60:429–446
- Friedrichs CT, Lynch DR, Aubrey DG (1992) Velocity asymmetries in frictionally-dominated tidal embayments: longitudinal and lateral variability. In: Prandle D (ed) Coastal and estuarine studies 40: dynamics and exchanges in estuaries and the coastal zone. American Geophysical Union, Washington DC, pp 277–312
- Gomes VJC, Freitas PTA, Asp NE (2013a) Dynamics and seasonality of the middle sector of a macrotidal estuary. *J Coast Res* SI65:1140–1145
- Gomes JD, Abrunhosa FA, Simith DJB, Asp NE (2013b) Mangrove sedimentary characteristics and implications for crab *Ucides cordatus* (Crustacea, Decapoda, Ucidiidae) distribution in an estuarine area of the Amazonian region. *Acta Amazon* 43:481–488
- Irion G, De Mello JASN, Morais J, Piedade MTF, Junk WJ, Garimig L (2010) Development of the Amazon valley during the middle to late quaternary: sedimentological and climatological observations. In: Junk WJ et al (eds) Amazonian floodplain forests: ecophysiology, biodiversity and sustainable management. Springer, Heidelberg, pp 27–42
- Lambiase JJ (1980) Hydraulic control of grain-size distributions in a macrotidal estuary. *Sedimentology* 27:433–446
- Lessa GC, Masselink G (1995) Morphodynamic evolution of a macrotidal barrier estuary. *Mar Geol* 129:25–46
- Mehlig U, Menezes MPM, Reise A, Schories D, Medina E (2010) Mangrove vegetation of the Caeté estuary. In: Saint-Paul U, Schneider H (eds) Mangrove dynamics and management in North Brazil. Springer, Heidelberg, pp 71–107
- Monteiro MC, Pereira LCC, Guimarães DO, Costa RAAM, Souza-Filho PWM, Vieira SR, Jiménez JA (2011) Influence of natural and anthropogenic conditions on the water quality of the Caeté river estuary (NE Brazil). *J Coast Res* SI64:1535–1539
- Moraes BC, Costa JMN, Costa ACL, Costa MH (2005) Variação espacial e temporal da precipitação no estado do Pará. *Acta Amazon* 35:207–214
- DHN - Diretoria de Hidrografia e Navegação, Marinha do Brasil (2015) <https://www.mar.mil.br/dhn/dhn/index.html>. Accessed 15 May 2015



- Nittrouer CA, Kuehl SA, Sternberg RW, Figueiredo AG Jr, Faria LEC (1995) Introduction to the geological significance of sediment transport and accumulation on the Amazon continental shelf. *Mar Geol* 125:177–192
- Pereira MD, Siegle E, Miranda LB, Schettini CAF (2010) Hidrodinâmica e transporte de material particulado em suspensão sazonal em um estuário dominado por maré: Estuário de Caravelas (BA). *Rev Bras Geofis* 28:427–444
- Pereira LCC, Vila-Concejo A, Short AD (2013) Influence of subtidal sand banks on tidal modulation of waves and beach morphology in Amazon macrotidal beaches. *J Coast Res* SI65:1821–1826
- Phillips JD (1991) Fluvial sediment delivery to a coastal plain estuary in the Atlantic drainage of the United States. *Mar Geol* 98:121–134
- Pianca C, Mazzini PLC, Siegle E (2010) Brazilian offshore wave climate based on NWW3 reanalysis. *Braz J Oceanogr* 58:53–70
- Schettini CAF, Miranda LB (2010) Circulation and suspended particulate matter transport in a tidally dominated estuary: Caravelas estuary, Bahia, Brazil. *Braz J Oceanogr* 58:1–11
- Siegle E, Schettini CAF, Klein AHF, Toldo EE Jr (2009) Hydrodynamics and suspended sediment transport in the Camboriú estuary—Brazil: pre jetty conditions. *Braz J Oceanogr* 57:123–135
- Silva CA, Souza Filho PWM, Rodrigues SWP (2009) Morphology and modern sedimentary deposits of the macrotidal Marapanim Estuary (Amazon, Brazil). *Cont Shelf Res* 29:619–631
- Souza Filho PWM, Lessa GC, Cohen MCL, Costa FR, Lara RJ (2009) The subsiding macrotidal barrier estuarine system of the Eastern Amazon coast, Northern Brazil. In: Dillenburg SF, Hesp PA (eds) *Geology and geomorphology of Holocene coastal barriers of Brazil*, 1st edn. Springer, New York, pp 347–376
- Speer PE, Aubrey DG, Friedrichs CT (1990) Nonlinear hydrodynamics of shallow tidal inlet/bay systems. In: Parker BB (ed) *Tidal hydrodynamics*. Wiley, New York, pp 321–339
- Uncles RJ, Stephens JA, Harris C (2006) Properties of suspended sediment in the estuarine turbidity maximum of the highly turbid Humber estuary system, UK. *Ocean Dyn* 56:235–247
- Wang ZB, Jeuken MCJL, Gerritsen H, de Vriend HJ, Kornman BA (2002) Morphology and asymmetry of the vertical tide in the Westerschelde estuary. *Cont Shelf Res* 22:2599–2609
- Wolanski E (1995) Transport of sediment in mangrove swamps. *Hydrobiologia* 295:31–42
- Wolanski E, Spagnol S (2003) Dynamics of the turbidity maximum in King Sound, tropical Western Australia. *Estuar Coast Shelf Sci* 56: 877–890